ADVANCED ENERGY MATERIALS
www.advenergymat.de

Sinter-Resistant Nickel Catalyst for Lignin Hydrogenolysis Achieved by Liquid Phase Atomic Layer Deposition of Alumina

*Farzaneh Talebkeikhah, Songlan Sun, and Jeremy S. Luterbacher**

Lignin hydrogenolysis is a key step in the sustainable production of renewable bio-based chemicals and fuels. Heterogeneous metal catalysts have led to high yields but they rapidly deactivate, notably due to nanoparticle sintering and carbonaceous deposit formation. While these deposits can be removed by regeneration, sintering is irreversible and a significant barrier to commercialization. Here, simple liquid phase atomic layer deposition is used to deposit an alumina layer to protect nickel particles from sintering. In the gas phase, it is proved that alumina can prevent sintering during reduction up to 600 °C. This catalyst for hydrogenolysis of extracted lignin in batch and continuous operation is used. In batch, the overcoated catalyst maintains high monomer yields with little sintering over four cycles of reuse while the yield obtained with the catalyst without an overcoat reduces to half and severe sintering occurs. In a continuous flow reactor, deactivation rates are three times lower for the catalyst with the alumina overcoat. Microscopy images confirm that the alumina overcoat largely preserves nickel particle sizes after ten days of operation. The results demonstrate that catalyst overcoating with metal oxides substantially slows irreversible deactivation during lignin hydrogenolysis, which could facilitate the development of continuous lignin upgrading.

1. Introduction

Biomass has received considerable attention as a sustainable source of carbon and alternative feedstock for fossil-based chemicals and fuels. Lignin, one of its three main components along with cellulose and hemicellulose, which are polysaccharides, has been the subject of increased research lately due to its low oxygen content and aromatic functionality. Due to this structure, lignin is more similar to many petrochemicals than other major biomass components especially polysaccharides. However, lignin is also especially complicated to exploit due to its tendency to irreversibly degrade during the initial biomass fractionation.[1,2] This degradation involves lignin condensation and the formation of highly stable interunit C—C linkages, that once formed, make selectively breaking down lignin into monoaromatic compounds difficult. Lignin from conventional biorefineries and paper making processes is especially recalcitrant to upgrading.

Recently, so-called lignin first strategies have emerged, which actively seek to prevent lignin degradation. One notable strategy called reductive catalytic fractionation (RCF), directly upgrades lignin during biomass fractionation by putting biomass or biomass extracts into contact with a reductant and a catalyst.[1,3–5] This process leads to the reduction and upgrading of reactive intermediates into stable monophenolics.[1,6] In this context, different types of catalysts like solid acids,[7] transition metal carbides,[8] metal sulfides,[9] porous metal oxides,[10] metal organic frameworks,[11] mono and bimetallic catalysts,[12] carbon based and other catalysts have been examined for lignin or lignin model compound hydrogenolysis.[13–16] Many studies have featured carbon-based catalysts because they generally feature better activity and stability compared to common metal oxide supported catalysts, that include those based on like alumina, silica, titania and aluminosilicates.[17–19]

An important challenge to scale all these processes is to achieve continuous and stable operation. Although Pd, Ru, and Ni on activated carbon (AC) displayed high yield in lignin hydrogenolysis[17,20] leaching, sintering, and surface poisoning are still key factors in limiting catalyst stability. For instance, Anderson et al. explored semi-continuous lignin upgrading by using flowthrough reactors that would rapidly send whole biomass extracts over supported metal catalysts in the presence of hydrogen. They observed severe Ni sintering of 50% increase in average diameter and 30% of leaching after processing 4 g of poplar wood over 12 h in their flow through reactor containing a single-bed of 15 wt% Ni/AC with a switchable biomass bed in upstream.[21] Other researchers have observed similar sintering. In batch hydrogenolysis, Park et al used 0.1 wt% Pd on N-doped carbon and core-shell Ni-alumina on activated carbon with 3 g of birch wood for 3 cycles. Although loss of activity

F. Talebkeikhah, S. Sun, J. S. Luterbacher
Laboratory of Sustainable and Catalytic Processing
Institute of Chemical Sciences and Engineering
École Polytechnique Fédérale de Lausanne (EPFL)
Station 6, Lausanne 1015, Switzerland
E-mail: jeremy.luterbacher@epfl.ch

The ORCID identification number(s) for the author(s) of this article can be found under https://doi.org/10.1002/aenm.202203377.

DOI: 10.1002/aenm.202203377

was not observed during these cycles but Ni particles agglomerated severely from 15 to 50 nm and nano clusters of Pd were formed.[22] In addition to carbon-based catalysts, sintering was reported for other types of supports. Ru sintered noticeably in Ni-Ru/HZSM-5 after hydrogenolysis of 0.4 g straw lignin at 230 °C.[23] Similarly Kasakov et al. noticed particle size increase of 0.4 nm for HZSM-5, 0.9 nm for SiO_2 and 1.5 nm for HBEA supported Ni catalyst after hydrogenolysis of 1 g organosolv lignin at 250 °C.[24] In the same manner sintering has been illustrated for Ni-Re/Nb_2O_5,[25] Rh/silica-alumina,[26] Ni/TiN,[27] Ni/CeO_2,[28] as well.

Recently, we have developed a lignin isolation process known as aldehyde assisted fractionation. This allows the extraction of a stabilized oligomeric form of lignin that can be isolated from the other biomass components, re-solubilized in an organic solvent and still be upgraded at high yields that are comparable to RCF. Isolating lignin before its reductive depolymerization avoids that other biomass fractions are exposed to the catalyst and reductant, which avoids unnecessary reactions and can protect the catalyst from harmful biomass-derived species including organic acids, which are thought to be responsible for much of the leaching seen with RCF.[21] Because the isolated aldehyde-stabilized lignin can be resolubilized in an organic solvent, it is also an ideal substrate for performing truly continuous upgrading in flow. We were recently able to demonstrate this steady-state continuous operation with a Ni/AC catalyst and propionaldehyde stabilized lignin.[17] However, in flow and after 3 cycles of hydrogenolysis catalyst deactivation was observed. Specifically when 3 g of lignin were processed over 200 h with 5 wt% Ni/AC, Ni nano particles sintered to more than twice of their initial size.[17]

In this work, we sought to improve continuous lignin upgrading by preparing a stabilized lignin hydrogenolysis catalyst, we successfully applied the simple liquid phase atomic layer deposition (ALD) for depositing alumina layer on activated carbon-based support. In contrast to gas phase ALD, this liquid phase ALD method uses common laboratory synthesis equipment and avoids the use of reactant excess and a purge cycle, while maintaining comparable coating quality to gas phase ALD.[29,30] Past work has shown that alumina deposition is a way to limit sintering during gas and liquid phase catalytic processing.[30–35] This liquid phase deposition method, developed recently in our group,[30] uses ligand titration to determine the exact quantity of reactant and counter reactant to be injected at each cycle, which leads to the reaction being self-limited by stoichiometry instead of a purge cycle. Here, we show that depositing an alumina overcoat over a Ni catalyst on a carbon support prevents Ni nanoparticle sintering and slows deactivation.

2. Results and Discussion

In stoichiometrically liquid phase ALD, reactive surface functional groups are crucial for initiating alumina deposition on the surface. However, physiosorbed water can also react and its presence inside activated carbon micropores can lead to a non-uniform deposition (Figure S1, Supporting Information). This issue can be addressed by removing the physiosorbed water by vacuum treatment of the substrate before alumina deposition.

We used Boehm titration to measure hydroxyl groups on commercial activated carbon (AC) and observed that the density of hydroxyl groups on the surface was 0.12 groups per nm^2 which was far less than surface hydroxyl groups of silica (2 OH nm^{-2}) that was successfully used as a substrate for liquid phase ALD in our previous work.[30] (Table S1, Supporting Information). This low density can lead to island growth of alumina, which in turn requires more injection cycles to have a protective layer on the catalyst.

To address this, we used concentrated nitic acid to oxidize the surface[31] and based on Boehm titration, total acid sites increased from 0.2 to 2.3 mmol g^{-1}. Also, X-ray photoelectron spectroscopy (XPS) spectra (Table S2, Figures S2–S5, Supporting Information) showed an increase in oxygen containing groups as well as nitrogen groups after treatment of commercial activated carbon with nitric acid. This treatment also reduced the surface area from 996 to 885 m^2 g^{-1} and pore volume from 0.96 to 0.78 cm^3 g^{-1} (Table S3, Figures S6 and S7, Supporting Information). Next, Ni was deposited on the nitric acid treated support using dry impregnation methods and the catalyst (Ni/AC) was then reduced at 450 °C overnight. This reduction decreased the amount of surface oxygen containing functional groups by reducing carboxylic functional groups to carbonyl or hydroxyl groups while reducing nickel oxide to nickel with hydrogen (Tables S1 and S2, Figures S2a, S3, and S4, Supporting Information). Moreover, after reduction at 450 °C, chemisorbed nitrogen oxide, created during nitric acid treatment on carbon surface was removed. However, different types of C—N bonds still existed on the surface of Ni/AC (Figure S2b, Supporting Information). In the end, to verify that this reduction had not substantially reduced surface oxygen groups, we titrated the surface of the catalyst with the first precursor, trimethyl aluminum (TMA), and compared ligand release with titration of untreated commercial activated carbon (Figure S8, Supporting Information). The higher slope and saturation point of the catalyst after Ni deposition and reduction, indicates that nitric acid treatment still is effective in increasing functional groups even after reduction at 450 °C. Assuming all methane released by the saturation point corresponds to surface hydroxyl groups reacting with TMA, we can estimate that a hydroxyl density of 0.55 OH nm^{-2} is present on the catalyst versus 0.13 OH nm^{-2} on the commercial activated carbon when TMA titration was used for quantification. However, this could be an underestimate due to steric hindrance of some hydroxyl groups.

Following this initial deposition, the surface was similarly titrated during other half cycles with either water or TMA (**Figure 1**b–d). After obtaining the required precursor quantity for the first 5 cycles, we observed that the amount of precursor needed for the 3rd, 4th, and 5th cycle was very similar, indicating that film growth was achieved (Figure 1d), which was consistent with our previous work.[30] Thus, by using the average quantity of precursors measured in the 3rd, 4th, and 5th cycle for the next 3 cycles, 8 layers of aluminum oxide were deposited on Ni/AC. The catalyst was then imaged with transmission electron microscopy before and after alumina deposition (Figure 1e–g), which showed that alumina was successfully deposited uniformly on the surface without any agglomeration.

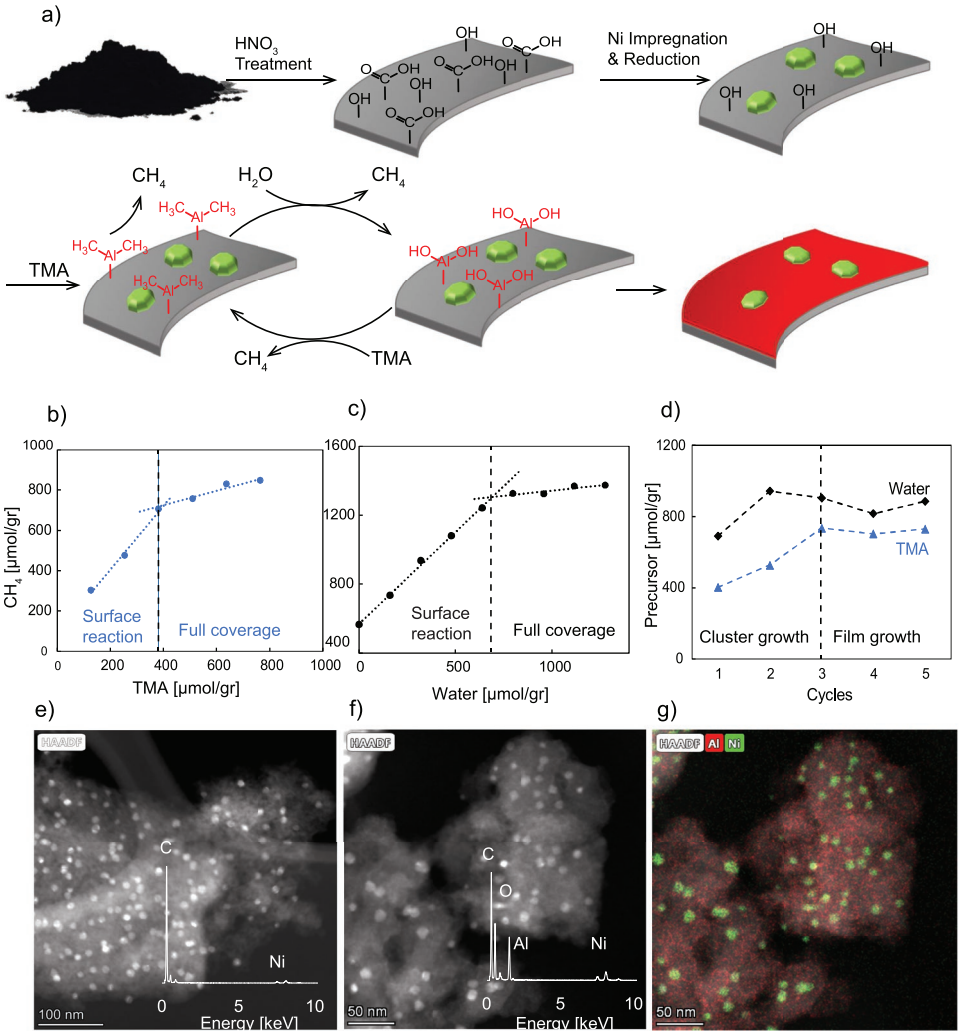

Figure 1. Catalyst synthesis by stoichiometrically limited liquid phase ALD. a) Schematic of the catalyst synthesis process. b) Surface titration with trimethyl aluminum (TMA) to find the stoichiometric quantity of TMA required to saturate the surface with alumina for the 1st half cycle. c) Surface titration with water to find the stoichiometric quantity of water to remove any remaining ligands during the 2nd half cycle. d) Stoichiometric quantity of precursor and counter reactant measured and added for each half cycle. e) High-angle annular dark-field (HAADF) image of Ni on activated carbon (Ni/AC) before alumina deposition with energy dispersive X-ray (EDX) spectrum f) HAADF image of Ni/AC after alumina deposition with EDX spectrum g) HAADF and EDX elemental mapping of Al@Ni/AC.

Once coated, we explored the ability of this overcoat to prevent Ni sintering in different conditions. First, with the help of H_2 chemisorption, we probed stability during thermal treatment. Since the Tamman temperature[36] for Ni is 591 °C, we exposed the catalyst twice to a stream of 10%H_2 in Ar at 600 °C for 1 h. Before and after each thermal test, we measured the adsorbed H_2 as an indication of available Ni surface. Since, the Ni content in 1 g of Al@Ni/AC is lower than Ni content in Ni/AC, these H_2 chemisorption tests were compared based on Ni mass (**Figure 2**a). Finally, particle size distributions were derived from transmission electron microscopic (TEM) images of the untreated and twice treated catalysts with and without alumina overcoat and compared with each other (Figure 2, Table S4, Supporting Information).

The reduction in chemisorbed H_2 for the uncoated Ni/AC, clearly shows the loss of Ni surface area due to sintering. In addition, TEM images and wider particle size distribution confirm sintering as large particles appear. Because of possible blockage of pores after alumina coating, the quantity of adsorbed H_2 on Al@Ni/AC was lower than the original catalyst. However, after thermal treatment, neither adsorbed H_2 nor particle size distribution substantially changed for this catalyst, which demonstrated the effectiveness of the coating in preventing sintering under these treatment conditions.

We also explored the effect of this overcoat in the harsh conditions associated with batch lignin hydrogenolysis (200 mg of propionaldehyde extracted lignin with catalyst, filled with 40 bar of H_2 and heated up to 250 °C for 3 h with tetrahydrofuran (THF) as the solvent). TEM imaging of spent catalysts after only one cycle of hydrogenolysis using high-angle annular dark-field (HAADF) mode and energy dispersive X-ray (EDX) elemental mapping, showed severe sintering for Ni/AC whereas no significant sintering was observed for the catalyst where alumina coating was present (**Figure 3**).

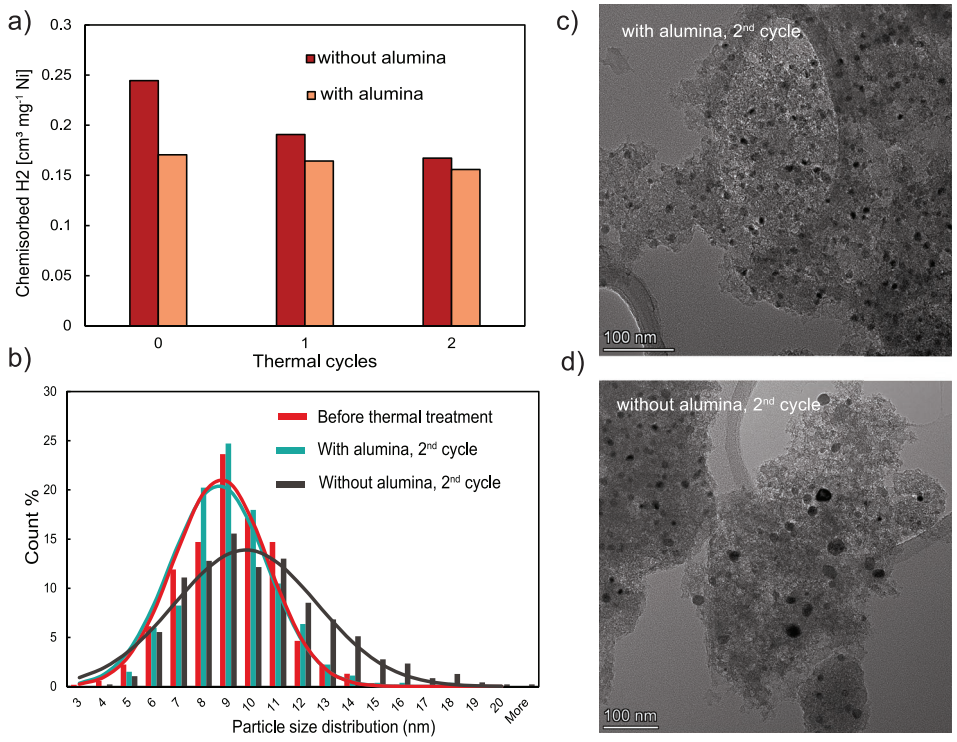

Figure 2. Thermal stability tests and overcoat effects. a) Chemisorbed H_2 before and after exposing the catalysts to 600 °C based on mass of Ni in each catalyst. b) Ni size distribution after 2 cycles of thermal exposure for both of the coated and uncoated catalysts. c) TEM image of Al@Ni/AC after 2 cycles of thermal treatment. d) TEM image of Ni/AC after 2 cycles of thermal treatment.

To confirm the effect of this apparent stabilization on yield, we separated and washed the catalysts after each use for use in a total of four batch lignin hydrogenolysis runs. To control the effect of condensate deposition on the catalyst surface, these tests were repeated but with a reduction of the catalysts at 450 °C after each batch reaction (**Figure 4**). After each reaction, lignin monomer yields were calculated based on monophenolic products quantified by gas chromatography with a flame ionization detector (GC-FID) and identified by a GC coupled to a mass spectrometer (GC-MS) (see Table S5 and Methods in the Supporting Information). Since the quantity of accessible Ni active sites on the coated catalyst was lower, due to possible blockage of the pores with alumina and increased mass of the catalyst after alumina deposition, is half of the uncoated catalyst (Table S4, Supporting Information), we compared the hydrogenolysis yields of 100 mg of Ni/AC with 200 mg of Al@Ni/AC.

The total monomer yield for both of the catalysts in the first run is the same indicating that the alumina layer didn't affect

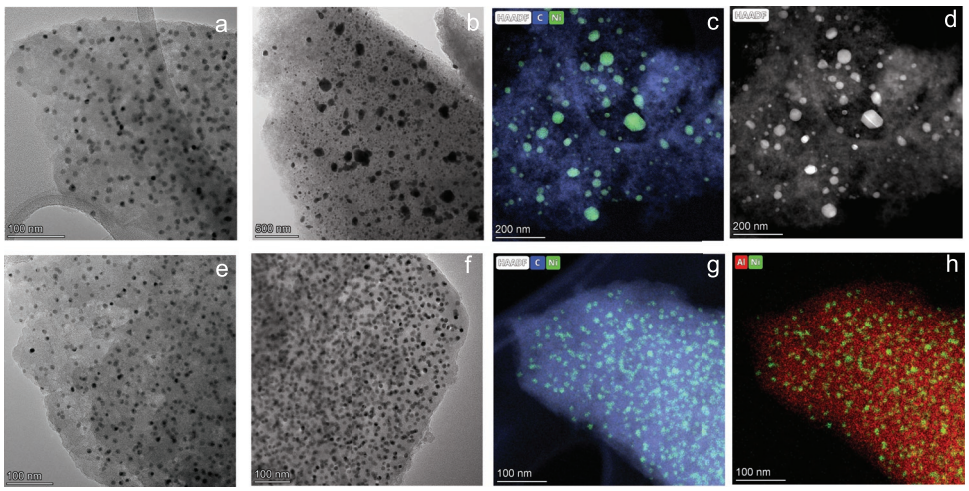

Figure 3. a) TEM image of Ni/AC before lignin hydrogenolysis. b–d) TEM, HAADF images, and EDX elemental mapping of Ni/AC after hydrogenolysis. e) TEM image of Al@Ni/AC before hydrogenolysis. f–h) TEM, HAADF images, and EDX elemental mapping of Al@Ni/AC after hydrogenolysis.

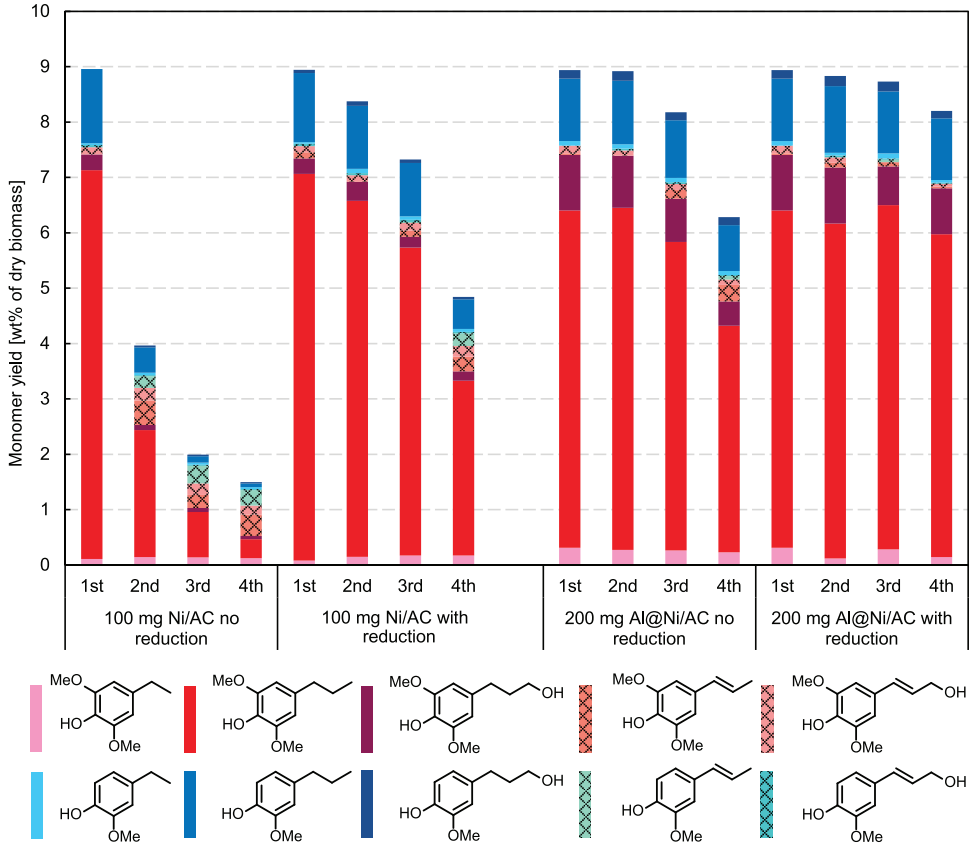

Figure 4. Catalyst recycling experiments for batch lignin hydrogenolysis with Ni/AC and Al@Ni/AC catalysts based on same nickel active site measured by H_2 chemisorption tests.

Ni activity to the point that maximum yields could not be achieved. Furthermore, the ratio of syringyl to guaiacyl-based monomers was very similar for both catalysts (5.3 for Ni/AC and 5.6 for Al@Ni/AC) which is consistent with the fact that this ratio is independent of the catalyst and depends primarily on the source of lignin and its extraction method.[37,38] There is a small difference in product selectivity, where the overcoated catalyst (Al@Ni/AC) appeared to preserve a greater fraction of terminal alcohol units on syringyl molecules leading to more 4-propanolsyringol (PSOH) being produced whereas with the Ni/AC catalyst, syringol units of lignin were cleaved and almost entirely hydrogenated to propyl syringol (PS). Over the next 3 runs, the Al@Ni/AC catalyst systematically exhibited a superior stability leading to preserved monomer yields whether or not a catalyst reduction was applied. The substantial drop in yield observed for runs with the overcoated catalyst when no reduction was used between runs was likely due to blocking of active sites by carbonaceous deposits derived from lignin. With a high temperature reduction, possible condensates were likely partially cleaved, solubilized or even gasified to lighter molecules such as CO, CO_2, CH_4.[39,40] Consequently, a substantial amount of these deposits was removed during this regeneration with the main remaining deactivation being associated with sintering. Thermogravimetric analysis (TGA) of Al@Ni/AC catalyst (Figure S10, Supporting Information) before and after reaction confirms formation of significant amount of condensates during hydrogenolysis of 200 mg of lignin. Moreover, these results show that reducing the catalyst at 450 °C after hydrogenolysis can remove considerable quantity of condensates which can help the catalyst retain its activity. However, TGA of the reduced catalyst (used for 4 times in hydrogenolysis with reduction in between) proves that even after reduction at 450 °C, not all the condensates are removed. For the catalyst without an alumina overcoat, although reduction removed deposits, the catalyst deactivated primarily because of sintering and the associated reduction in Ni surface. To correlate the reduction in lignin hydrogenolysis activity with the quantity of surface nickel, we carried out this process with different quantities of Ni/AC catalysts. Using dispersions estimated from particle size distributions obtained by TEM images (Table S6, Supporting Information), we calculated the corresponding amount of nickel surface sites and compared this number with the resulting lignin hydrogenolysis activity when different quantities of Nickel surface sites were present during the reaction by changing the catalyst mass or nickel dispersion (Figure S11, Supporting Information). After the first run, Ni dispersion on Ni/AC reduced from 14.2% to 9.4% representing a nickel surface reduction from 0.153 to 0.101 µmol mg^{-1}. Based on Figure S11 (Supporting Information), 0.101 µmol mg^{-1} of available nickel surface for 100 mg Ni/AC leads to about 9% monomer yield (dry biomass basis) which is comparable to the monomer yield actually obtained in the second run with recycled Ni/AC (Figure 4). This comparison indicates that sintering, i.e., loss of Ni surface was the primary reason for the loss in monophenolic monomer yield.

For the runs that did not feature a regeneration, Al@Ni/AC led to better activity than Ni/AC. In Figure 4, the Al@Ni/AC catalyst loading was higher to maintain the same number of active sites as measured by H_2 chemisorption. However, even when performing runs based on using the same Ni loading in all runs, Al@Ni/AC outperformed the recycled uncoated catalyst and led to higher monomer yields in all the cycles (Figure S12, Supporting Information).

We systematically measured whether Ni and Al had leached into solution with Inductively Coupled Plasma (ICP) tests. (Table S7, Supporting Information). For both of the catalysts, the amount of leached Ni and Al to the solution was negligible with respect to the initial Ni and Al content in the catalysts and comparable to the quantity of these elements already present in the lignin. Nevertheless, for Al@Ni/AC, the amount of nickel detected in solution after the reaction was about 10 times lower than for Ni/AC catalyst, which demonstrates the stabilizing effect of the overcoat.

The phases of the various materials present in these catalysts were characterized and compared before and after reactions with X-Ray diffraction spectrometry (XRD, Figure S13, Supporting Information). In all cases, a metallic nickel phase was detected, which was expected given the pressurized H_2 gas being present during reaction. Simultaneously, for the Ni/AC catalyst, we observed additional crystalline peaks after the fourth run that could not be attributed to nickel or alumina. These peaks are likely related to impurities, which exist inside lignin and are adsorbed and accumulated on the surface of the catalyst over 4 consecutive batch reactions. Based on ICP experiments, lignin itself has impurities, notably inorganic salts, that likely originate from wood and that end up with lignin during the fractionation procedure (Table S8, Supporting Information). Ca is the main element present in the lignin fraction. Other impurities containing Fe, K, Mg were detected as well. Furthermore, these impurities were measured for the catalysts before and after hydrogenolysis (Table S9, Supporting Information). For both catalysts, we measured a significant increase in these elements after the hydrogenolysis cycles, demonstrating the catalyst's propensity to accumulate these inorganic species.

Microscopy images were taken after the 4th cycle and the particle size distribution was measured before the 1st and after the 4th cycle. Based on particle size distribution (Figure S14, Supporting Information), the alumina overcoat after 4 cycles of hydrogenolysis protected Ni particles to some extent and no severe growth was observed, whereas significant growth was observed without the overcoat present. We observed particles as large as micron size after 4 cycles with Ni/AC (Figure S15, Supporting Information). We even observed isolated Ni particles that had detached from the support. Furthermore, particles of impurities, mainly Ca, were formed on the catalyst surface which was consistent with the additional peaks observed with XRD confirming that impurities formed crystalline species during these cycles of hydrogenolysis on Ni/AC. For Al@Ni/AC (Figure S16, Supporting Information), despite the EDX spectrum revealing existence of impurities on the surface, nanoparticles of impurities were not formed on the surface without the overcoat. Presumably, this can be attributed to alumina defect sites anchoring the impurities.[41–43]

To better understand the reason for the low-level sintering that was observed during multiple recycles with Al@Ni/AC catalyst (i.e., after 4 consecutive cycles of hydrogenolysis), we repeated batch hydrogenolysis with Al@Ni/AC without any reactants for 4 cycles. Unlike the case where lignin was present (Figure S16, Supporting Information), for the case without lignin, the particle size distribution didn't change, which points to the key role of lignin in sintering of Ni particles (Figure S17, Supporting Information). Considering the dominant effect of lignin in sintering and the fact that with the Ni/AC catalyst, we observed Ni particles was detached from the surface of the catalyst after 4th run, we can presume that Ni adatoms at high temperatures form metal-reactant complexes (probably with oxygen containing functional groups of lignin) leading to disintegration and eventually separation of nickel adatoms from catalyst surface.[44] This metalorganic formation between metallic active sites and reactants during a reaction has been reported elsewhere.[45–49]

To even prevent this low level of sintering in Al@Ni/AC after 4 cycles of hydrogenolysis, we tried to change the reaction conditions. Previously with all batch hydrogenolysis, the reaction was stopped by fast cooling down with compressed air (in less than 10 min the reaction temperatures dropped from 250 to below 100 °C). We changed the reaction conditions and we let the reaction to cool down by itself. To verify the cooling rate effect, 4 cycles of batch hydrogenolysis with a catalyst reduction in between were repeated again for Al@Ni/AC but this time with slower rate of stopping and cooling down the reaction (in less than 1 h the reaction temperature dropped from 250 to below 100 °C). HAADF, EDX images (Figure S18, Supporting Information) and corresponding particle size distribution (Figure S19, Supporting Information) clearly shows the advantageous effect of slower cooling down in preventing sintering completely. This effect was examined for Ni/AC without alumina as well. From microscopic images, after only one cycle of hydrogenolysis, (Figure S20, Supporting Information), slower cooling rate didn't prevent sintering and also compared to the case with fast cooling rate, significantly bigger Ni particles were formed.

From these results, the sintering mechanism during lignin hydrogenolysis is complicated and not yet been resolved and further research are necessary to understand the role of lignin–nickel interaction. We hypothesize that a slower cooling rate may give time to the Ni in the Ni-lignin complexes to re-adsorb on defect sites within the overcoat as the temperature drops. In summary, with the alumina layer we prevented major sintering and with a slower cooling rate, we were able to prevent sintering completely in consecutive batch lignin hydrogenolysis runs.

Ultimately, lignin hydrogenolysis will have to be done continuously and likely in flow to achieve commercialization. For this reason, we also evaluated this triphasic process in a flow reactor. Flow conditions also enable a better characterization of deactivation, especially when running at less than full yield. Based on our previous work,[17] we first started with the same condition of 200 mg Al@Ni/AC, 180 °C, 60 bar, 0.1 mL min^{-1} liquid flow rate and 50 mL min^{-1} STP H_2 gas. For the liquid feed, we used methanol as a solvent due to its improved performance at lower temperature (at 250 °C in batch conditions,

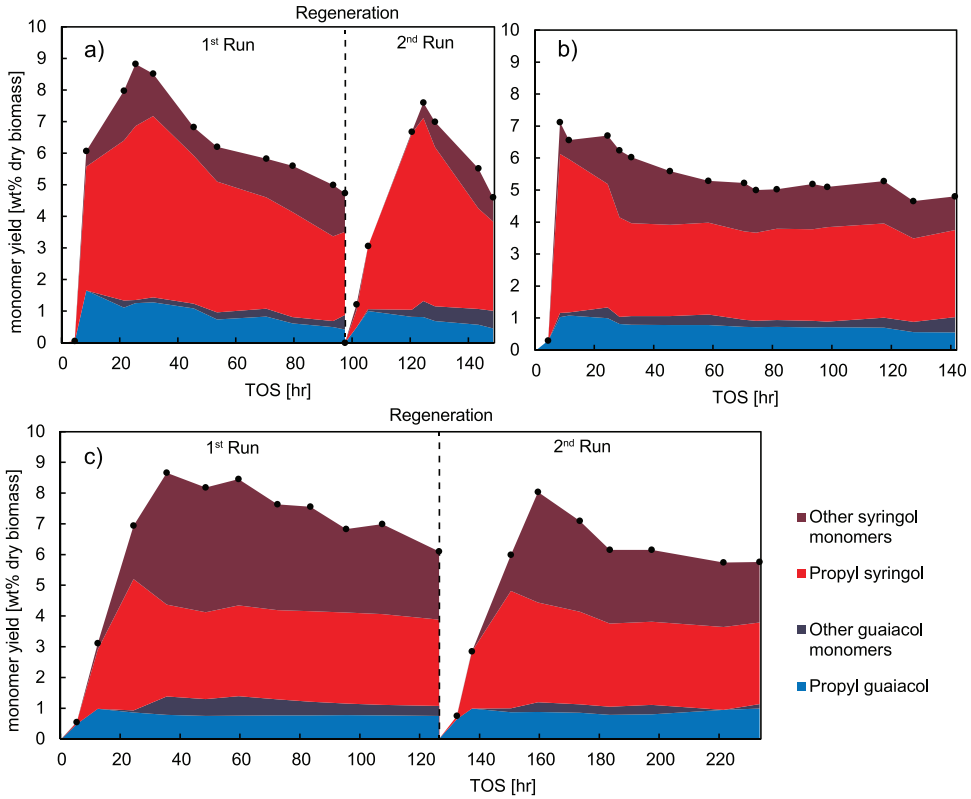

Figure 5. Continuous lignin hydrogenolysis at 200 °C, at 60 bar with 17 mL min^{-1} H_2 and a 0.1 mL min^{-1} liquid flow rate respectively (4:1 v/v methanol: dioxane) with 2.5 mg mL^{-1} lignin. a) 100 mg Ni/AC, b) 200 mg Al@Ni/AC, c) 300 mg Al@Ni/AC.

the choice of solvent had little effect on yield or selectivity, Figure S21, Supporting Information). However, since methanol doesn't completely dissolve propionaldehyde stabilized-lignin we used a mixture of dioxane and methanol (80:20% volume methanol to dioxane) to avoid clogging. Despite high monomer yields in batch hydrogenolysis for Al@Ni/AC, in continuous mode, we did not observe high monomer yields in the exiting stream (Table S10, Supporting Information). In an attempt to find a suitable operational condition for Al@Ni/AC, we tried reducing H_2 gas flow from 50 to 17 mL min^{-1}, which led to a sharp increase in monomer yield (Table S11, Supporting Information). Using these conditions, we were able to reach lignin monomer yields that were comparable to batch conditions (between 8 and 9% based on the initial dry biomass). After 4 h of operation we detected a high molecular weight compound with a noticeable peak at higher retention time in the GC spectrum (Figure S22, Supporting Information). We measured the protonated molecular weight of this compound with high resolution electrospray ionization mass spectroscopy (HR-ESI-MS), which was 387.1807 g mol^{-1}. This weight matches the chemical formula of $C_{22}H_{26}O_6$, which may be related to β–β structure of lignin. Interestingly, by increasing the reaction temperature from 180 to 200 °C, this high molecular weight compound was no longer present in the products observable by GC-FID suggesting it may be cleaved or degrade. Separation of this compound was tricky and thus determining its exact structure was deemed beyond the scope of the current effort.

As a control, these conditions (200 °C and 17 mL min^{-1} STP H_2 gas) were then used for 100 mg of Ni/AC for continuous lignin hydrogenolysis (**Figure 5**a, Table S12, Supporting Information). Using the uncoated catalyst, we reached a maximum yield, which was comparable to batch conditions, after 20 h. Then catalyst activity gradually reduced from above 8% to 5% after 90 h. This time on stream (TOS) corresponds to the processing of 13.5 g lignin per g of catalyst, which is more than what was processed in 4 cycles of batch experiments (8 g of lignin processed per g catalyst). Another way of comparing batch and continuous operation is to compare the turnover number (TON) using the number of monophenolic molecules produced and the exposed Ni sites measured through chemisorption. In this case, the TON is 106 for the flow reactor versus 80 for 4 cycles of batch hydrogenolysis. Just as we saw in batch experiments, we also see a similar drop but with a slower rate in activity in flow reactor (9.4 vs 3.3 [wt% monomers of original lignin] drop in yield over 4 batch cycles vs in the flow reactor, respectively).

Since some of this deactivation is likely due to carbonaceous deposits from lignin, we applied the same regeneration method used in batch mode. After letting the column to cool down to room temperature under 17 mL min^{-1} H_2 gas flow, we flushed the catalyst with 0.3 mL min^{-1} solvent (4:1 methanol to dioxane) for 3 h and then we reduced the catalyst again at 450 °C. We collected and concentrated the washing solvent to get some insight into material that might adsorb on the catalyst, which could be a precursor to carbonaceous deposits and analyzed this solution

by GC-MS (Figure S23, Supporting Information). Based on GC-MS, this darkly colored solution contained monophenolic compounds plus other high molecular weight compounds. After regeneration, the initial yield again reached over 8wt% but was followed by a higher deactivation rate (3wt%/day drop in yield relative to 1.4 wt%/ day before regeneration).

When using 200 mg of Al@Ni/AC, which corresponded to the same quantity of Ni active sites as the uncoated catalyst based on H_2 chemisorption, (Figure 5b, Tables S13 and S4, Supporting Information), the maximum yield was slightly lower (7% monomers, dry biomass basis). However, the catalyst deactivated more slowly than Ni/AC (0.4 wt%/day, 8 times more slowly than without the overcoat) and even appeared relatively stable after 50 h time-on-stream. Even though the use of Al@Ni/AC did not lead to the maximum attainable monomer yield, the turnover number achieved for Al@Ni/AC was still higher than for Ni/AC, when considering both runs up to the point where 5% yield was reached ($TON_{Al@Ni/AC}$:134 and $TON_{Ni/AC}$:106). Since we saw a clear regeneration effect when performing a reduction in batch, and because we observed a gradual pressure increase within the flow reactor that was likely indicative of condensation, we performed regeneration tests. We tested both regeneration and the effect of higher catalyst loadings with the overcoated catalyst by using 300 mg of Al@Ni/AC (Figure 5c, Table S14, Supporting Information). We hypothesized that this higher loading may facilitate reaching the maximal yield (i.e., above 8%, which is comparable with the uncoated catalyst). With this loading, higher monomer yields were indeed achieved and were comparable to those obtained with 100 mg of Ni/AC. However, the catalyst also seemed to deactivate faster at this higher loading, though still more over twice as slowly (0.6 wt% day^{-1}) than for the uncoated catalyst (1.4 wt% day^{-1}). Next, the catalyst was flushed with solvent and regenerated in the same was as for Ni/AC regeneration. In contrast to what we saw with Ni/AC, the resulting washing solution obtained with Al@Ni/AC contained less detectable complex material (Figure S24, Supporting Information).

The ratio of syringyl to guaiacyl-based products at maximum yield was very similar for both the alumina-coated (5.3) and uncoated catalyst (5.5) and equal to the derived ratio from batch experiments. Interestingly, in continuous mode, propyl syringol selectivity was lower than its selectivity in batch mode which could be due to the difference in residence time and operating temperature. In addition, similarly to batch results, selectivity for other syringyl monomers notably propanol syringol was higher with the alumina coated catalyst than uncoated Ni/AC.

Interestingly, these flow processes took fairly long to reach maximal yields (up to 30 h). In fact, the first samples that were collected after several hours were very dilute and sometimes contained almost no lignin derived molecules. This long time required to reach steady-state operation (Figure S25, Supporting Information) likely had to do with the time it took for a stable flow pattern and wetting occurring over the catalyst. We speculate that this is the case because steady state can be accelerated by flushing the catalyst with solvent prior to introducing the lignin feed (Table S15, Figure S26, Supporting Information). Similar to batch reactions, after the 2nd run, the catalysts were collected and microscopy images were taken from them. Based on HAADF, EDX images (Figure S27, Supporting Information) and particle size distribution (Figure S29, Supporting Information), nickel particle size for Al@Ni/AC catalyst after 10 days of operation didn't change and particles of impurities didn't form on the surface as well. However, since this catalyst was collected directly after 2nd run, without any regeneration, we can also see condensed lignin inside the catalyst. for the Ni/AC catalyst, significant sintering was observed after 5 days of operation and particles of impurities as well as isolated nickel particles were formed (Figures S28–S29, Supporting Information). Leaching of nickel and aluminum was also investigated and confirmed to be negligible for the coated catalyst in the flow reactor (Table S16, Supporting Information). Similar to what we saw in batch operation, the low quantity of detected Ni and Al was comparable to the quantity of Al or Ni that could be detected in the lignin itself which means that we cannot even attribute these small quantities to leaching from the catalyst.

3. Conclusions

Sintering and catalyst restructuring is a common challenge in lignin or biomass hydrogenolysis. Here we used a simple liquid phase atomic layer deposition method to overcoat a Ni/AC catalyst with an alumina overcoat and we demonstrated the effectiveness of this layer in preventing sintering of nickel particles in gas phase, batch and continuous lignin hydrogenolysis. Hydrogen chemisorption and microscopic images clearly shows the effectiveness of alumina layer in preventing sintering in gas phase. Higher monomer yields confirmed the superior stability of the coated catalyst relative to the uncoated one over 4 cycles of batch hydrogenolysis. Although, compared to Ni/AC, low level of sintering was observed for Al@Ni/AC after 4 cycles of hydrogenolysis, this low sintering could be eliminated by changing the reaction condition. By cooling down the reactors very slowly, with Al@Ni/AC we can completely protect Ni particles from sintering. Likewise, in continuous lignin hydrogenolysis, with alumina coated catalyst, based on same Ni active sites, deactivation rates reduced to one third of the rates for the case without alumina coating. Additionally, microscopic images verified the effectiveness of alumina coating in protecting Ni particles in continuous mode in the same way as for batch runs. This work demonstrates that catalyst overcoating could be an important tool in maintaining high catalyst activity during processing of renewable substrates such as lignin and therefore facilitate the industrial development of catalytic biomass upgrading.

Supporting Information

Supporting Information is available from the Wiley Online Library or from the author.

Acknowledgements

This work was supported by the European Research Council (ERC) under the European Union's Horizon 2020 research and innovation

program (Grant: CATACOAT, No 588251) and by EPFL. The authors wish to acknowledge Wu Lan for training to use Parr and Flow reactors, Mounir Driss Mensi for XPS, and Sylvain Coudret for ICP measurements respectively.

Conflict of Interest

The authors declare no conflict of interest.

Author Contributions

F.T. and J.S.L. conceived the project. F.T. performed synthesis, catalytic tests, microscopy, XRD, TGA, surface characterizations. S.S. performed flash chromatography and HRMS.

Data Availability Statement

The data that support the findings of this study are available from the corresponding author upon reasonable request.

Keywords

activated carbon, catalyst regeneration, defect sites, reductive catalytic fractionation, sintering

Received: October 6, 2022
Revised: December 23, 2022
Published online:

[1] M. M. Abu-Omar, K. Barta, G. T. Beckham, J. S. Luterbacher, J. Ralph, R. Rinaldi, Y. Román-Leshkov, J. S. M. Samec, B. F. Sels, F. Wang, *Energy Environ. Sci.* **2021**, *14*, 262.
[2] Y. M. Questell-Santiago, M. V. Galkin, K. Barta, J. S. Luterbacher, *Nat. Rev. Chem.* **2020**, *4*, 311.
[3] S. Van Den Bosch, W. Schutyser, R. Vanholme, T. Driessen, S.-F. Koelewijn, T. Renders, B. De Meester, W. J. J. Huijgen, W. Dehaen, C. M. Courtin, B. Lagrain, W. Boerjan, B. F. Sels, *Energy Environ. Sci.* **2015**, *8*, 1748.
[4] J. M. Pepper, H. Hibbert, *J. Am. Chem. Soc.* **1948**, *70*, 67.
[5] J. H. Jang, D. G. Brandner, R. J. Dreiling, A. J. Ringsby, J. R. Bussard, L. M. Stanley, R. M. Happs, A. S. Kovvali, J. I. Cutler, T. Renders, J. R. Bielenberg, Y. Román-Leshkov, G. T. Beckham, *Joule* **2022**, *6*, 1859.
[6] T. Renders, G. Van Den Bossche, T. Vangeel, K. Van Aelst, B. Sels, *Curr. Opin. Biotechnol.* **2019**, *56*, 193.
[7] W. Guan, C.-W. Tsang, C. S. Ki Lin, C. Len, H. Hu, C. Liang, *Bioresour. Technol.* **2020**, *298*, 122432.
[8] H. Guo, Bo Zhang, C. Li, C. Peng, T. Dai, H. Xie, A. Wang, T. Zhang, *ChemSusChem* **2016**, *9*, 3220.
[9] K. Wu, W. Wang, H. Guo, Y. Yang, Y. Huang, W. Li, C. Li, *ACS Energy Lett.* **2020**, *5*, 1330.
[10] G. Warner, T. S. Hansen, A. Riisager, E. S. Beach, K. Barta, P. T. Anastas, *Bioresour. Technol.* **2014**, *161*, 78.
[11] Q. Wang, T. Su, Yu Wang, Y. Chen, X. Lu, R. Ma, Y. Fu, W. Zhu, *ACS Sustainable Chem. Eng.* **2020**, *8*, 17008.
[12] T. Li, Na Ji, Z. Jia, X. Diao, Z. Wang, Q. Liu, C. Song, X. Lu, *ChemCatChem* **2020**, *12*, 5288.
[13] H. Zhang, S. Fu, Xu Du, Y. Deng, *ChemSusChem* **2021**, *14*, 2268.
[14] A. Shivhare, D. Jampaiah, S. K. Bhargava, A. F. Lee, R. Srivastava, K. Wilson, *ACS Sustainable Chem. Eng.* **2021**, *9*, 3379.
[15] X. Wang, M. Arai, Q. Wu, C. Zhang, F. Zhao, *Green Chem.* **2020**, *22*, 8140.
[16] P. Sudarsanam, R. Zhong, S. Van Den Bosch, S. M. Coman, V. I. Parvulescu, B. F. Sels, *Chem. Soc. Rev.* **2018**, *47*, 8349.
[17] Wu Lan, Y. P. Du, S. Sun, J. Behaghel De Bueren, F. Héroguel, J. S. Luterbacher, *Green Chem.* **2021**, *23*, 320.
[18] Qi Song, F. Wang, J. Cai, Y. Wang, J. Zhang, W. Yu, J. Xu, *Energy Environ. Sci.* **2013**, *6*, 994.
[19] E. Osamudiamhen Ebikade, N. Samulewicz, S. Xuan, J. D. Sheehan, C. Wu, D. G. Vlachos, *Green Chem.* **2020**, *22*, 7435.
[20] Y. Li, B. Demir, L. M. Vázquez Ramos, M. Chen, J. A. Dumesic, J. Ralph, *Green Chem.* **2019**, *21*, 3561.
[21] E. M. Anderson, M. L. Stone, R. Katahira, M. Reed, G. T. Beckham, Y. Román-Leshkov, *Joule* **2017**, *1*, 613.
[22] J. Park, U. Mushtaq, J. R. Sugiarto, D. Verma, J. Kim, *Appl. Catal., B* **2022**, *310*, 121280.
[23] F. Lin, Y. Ma, Y. Sun, K. Zhao, T. Gao, Y. Zhu, *Renewable Energy* **2021**, *170*, 1070.
[24] S. Kasakov, H. Shi, D. M. Camaioni, C. Zhao, E. Baráth, A. Jentys, J. A. Lercher, *Green Chem.* **2015**, *17*, 5079.
[25] L. Kong, L. Zhang, J. Gu, Le Gou, L. Xie, Y. Wang, L. Dai, *Bioresour. Technol.* **2020**, *299*, 122582.
[26] Ji. S. Yoon, J.-W. Choi, D. J. Suh, K. Lee, H. Lee, J.-M. Ha, *ChemCatChem* **2015**, *7*, 2669.
[27] L.-L. Bie, F.-J. Liu, Z.-M. Zong, G.-H. Liu, J.-P. Guo, Z.-X. Li, Z.-H. Ma, W.-W. Yan, X.-Y. Wei, *Fuel Process. Technol.* **2020**, *209*, 106523.
[28] W. Schutyser, S. Van Den Bosch, J. Dijkmans, S. Turner, M. Meledina, G. Van Tendeloo, D. P. Debecker, B. F. Sels, *ChemSusChem* **2015**, *8*, 1805.
[29] P. O. Oviroh, R. Akbarzadeh, D. Pan, R. A. M. Coetzee, T.-C. Jen, *Sci. Technol. Adv. Mater.* **2019**, *20*, 465.
[30] B. P. Le Monnier, F. Wells, F. Talebkeikhah, J. S. Luterbacher, *Adv. Mater.* **2019**, *31*, 1904276.
[31] J. Lu, B. Fu, M. C. Kung, G. Xiao, J. W. Elam, H. H. Kung, P. C. Stair, *Science* **2012**, *335*, 1205.
[32] B. J. O'neill, D. H. K. Jackson, A. J. Crisci, C. A. Farberow, F. Shi, A. C. Alba-Rubio, J. Lu, P. J. Dietrich, X. Gu, C. L. Marshall, P. C. Stair, J. W. Elam, J. T. Miller, F. H. Ribeiro, P. M. Voyles, J. Greeley, M. Mavrikakis, S. L. Scott, T. F. Kuech, J. A. Dumesic, *Angew. Chem., Int. Ed.* **2013**, *52*, 13808.
[33] B. J. O'neill, D. H. K. Jackson, J. Lee, C. Canlas, P. C. Stair, C. L. Marshall, J. W. Elam, T. F. Kuech, J. A. Dumesic, G. W. Huber, *ACS Catal.* **2015**, *5*, 1804.
[34] F. Héroguel, B. P. Le Monnier, K. S. Brown, J. C. Siu, J. S. Luterbacher, *Appl. Catal., B* **2017**, *218*, 643.
[35] F. Héroguel, L. Silvioli, Y.-P. Du, J. S. Luterbacher, *J. Catal.* **2018**, *358*, 50.
[36] Y. Dai, P. Lu, Z. Cao, C. T. Campbell, Y. Xia, *Chem. Soc. Rev.* **2018**, *47*, 4314.
[37] M. Talebi Amiri, G. R. Dick, Y. M. Questell-Santiago, J. S. Luterbacher, *Nat. Protoc.* **2019**, *14*, 921.
[38] Wu Lan, M. T. Amiri, C. M. Hunston, J. S. Luterbacher, *Angew. Chem.* **2018**, *130*, 1370.
[39] W. Yin, M. V. Alekseeva (Bykova), R. H. Venderbosch, V. A. Yakovlev, H. J. Heeres, *Energies* **2020**, *13*, https://doi.org/10.3390/en13010285.
[40] J.-Y. Kim, H. Hwang, S. Oh, Y.-S. Kim, U.-J. Kim, J. W. Choi, *Int. J. Biol. Macromol.* **2014**, *66*, 57.
[41] Y. Zhang, Y. Zu, D. He, J. Liang, L. Zhu, Yi Mei, Y. Luo, *Appl. Catal., B* **2022**, *315*, 121539.
[42] W. Han, B. Liu, Y. Chen, Z. Jia, X. Wei, W. Song, *J. Catal.* **2021**, *400*, 255.
[43] H. Chen, C. Fang, X. Gao, G. Jiang, X. Wang, S.-P. Sun, W. Duo Wu, Z. Wu, *J. Colloid Interface Sci.* **2021**, *581*, 964.

[44] R. Ouyang, J.-X. Liu, W.-X. Li, *J. Am. Chem. Soc.* **2013**, *135*, 1760.
[45] Y. Bai, J. Zhang, G. Yang, Q. Zhang, J. Pan, H. Xie, X. Liu, Y. Han, Y. Tan, *ACS Catal.* **2018**, *8*, 6367.
[46] B. R. Goldsmith, E. D. Sanderson, R. Ouyang, W.-X. Li, *J. Phys. Chem. C* **2014**, *118*, 9588.
[47] S. Hu, R. Ouyang, W.-X. Li, *J. Energy Chem.* **2019**, *30*, 108.
[48] G. Yan, Yu Tang, Y. Li, Y. Li, L. Nguyen, T. Sakata, K. Higashi, F. F. Tao, P. Sautet, *Nat. Catal.* **2022**, *5*, 119.
[49] Q. Wan, F. Wei, Y. Wang, F. Wang, L. Zhou, S. Lin, D. Xie, H. Guo, *Nanoscale* **2018**, *10*, 17893.